DEVELOPMENTAL BIOLOGY

Tenascin-C expressing touch dome keratinocytes exhibit characteristics of all epidermal lineages

Minh Binh Nguyen[1]†, Pooja Flora[1]†, Meagan C. Branch[1], Madison Weber[1], Xiang Yu Zheng[2,3], Unnikrishnan Sivan[4]‡§, Simon Joost[4]¶, Karl Annusver[4,5], Deyou Zheng[2,3], Maria Kasper[4,5], Elena Ezhkova[1]*

The touch dome (TD) keratinocytes are specialized epidermal cells that intimately associate with the light touch sensing Merkel cells (MCs). The TD keratinocytes function as a niche for the MCs and can induce de novo hair follicles upon stimulation; however, how the TD keratinocytes are maintained during homeostasis remains unclear. scRNA-seq identified a specific TD keratinocyte marker, *Tenascin-C* (TNC). Lineage tracing of *Tnc*-expressing TD keratinocytes revealed that these cells maintain themselves as an autonomous epidermal compartment and give rise to MCs upon injury. Molecular characterization uncovered that, while the transcriptional and chromatin landscape of the TD keratinocytes is remarkably similar to that of the interfollicular epidermal keratinocytes, it also shares certain molecular signatures with the hair follicle keratinocytes. Our study highlights that the TD keratinocytes in the adult skin have molecular characteristics of keratinocytes of diverse epidermal lineages.

INTRODUCTION

Sensory perception acts as a connection between our internal and external worlds and is divided into five major senses that help us navigate through our surroundings. More specifically, somatosensory function allows us to perceive temperature, pain, and touch by connecting the skin to the central nervous system via mechanoreceptors located in the epidermis and sensory nerves (*1*–*3*). On the surface of the skin, receptors perceive light touch sensations, which allow us to interpret objects and manipulate body dexterity (*4*). Thus, dissecting the dynamics, function, and molecular characteristics of the mechanosensory niche in the skin is imperative for understanding the regulation and maintenance of light touch sensation. The mechanosensory touch dome (TD) niche in the skin surrounds primary hair follicles (HFs) and is composed of specialized keratinocytes, known as TD keratinocytes, and Merkel cells (MCs). MCs are responsible for light touch detection, while the TD keratinocytes stand as a separate innervated structure directly above the MCs (*4*, *5*). In developing murine mammals, TD keratinocytes arise from the hair placode and appear as a keratin (KRT) 17–positive ($KRT17^+$) structure independent of the developing HF by embryonic day 16.5 (E16.5) (*6*). At the same time, $KRT8^+$ MCs shift their position from the developing HF to localize beneath the TD cells in the interfollicular epidermis (IFE) (*6*). Once the mechanosensory niche is established, however, the source of TD maintenance remains unclear.

The function of the TD keratinocytes has been studied mostly during early development where these cells have been shown to be critical for patterning MC innervation (*6*–*8*). In the adult skin, TD keratinocytes are critical for TD innervation and MC maintenance (*9*); however, whether these cells give rise to MCs is a subject of debate. TD keratinocytes can acquire a HF fate and form de novo HFs upon an increase of hedgehog signaling driven by *Ptch1* knockdown (*10*). What molecular characteristics of TD keratinocytes allow for these diverse properties is unknown.

Here, we identified and established a previously unidentified TD keratinocyte marker, *Tenascin-C* (TNC), to further investigate the potential and function of TD keratinocytes during adult skin homeostasis. By conducting lineage tracing experiments using *Tnc-CreER; $R26^{tdTomato}$* mice, we found that TNC expressing (TNC^+) TD cells undergo self-renewal in unison with hair cycle activation and function as an autonomous self-maintaining epidermal compartment. TNC^+ TD keratinocytes do not give rise to MCs during normal homeostasis but can replenish MCs upon injury. High-throughput transcriptional and chromatin analyses uncovered that the molecular landscape of TNC^+ TD keratinocytes is very similar to IFE cells and that TNC^+ TD keratinocytes can occasionally acquire the IFE basal keratinocyte fate as the mice age. Intriguingly, TNC^+ TD keratinocytes express many HF stem cell (HFSC) genes and maintain open chromatin regions associated with HF; however, they do not arise from the HFs in the homeostatic adult skin. Together, this suggests that TD keratinocytes are an autonomous cell compartment that is primed to give rise to diverse epidermal lineages in the adult skin.

RESULTS

TNC is expressed in the TD keratinocytes of the adult dorsal skin

To identify TD keratinocyte signature genes in the adult skin, we conducted single-cell RNA sequencing (scRNA-seq). We used postnatal 50 (P50) *Gli1-$CreER^{T2}$; $Rosa26^{tdTomato}$* mice, in which the TD keratinocytes and a subset of HF bulge cells get efficiently labeled under *Gli1*-promoter control (Fig. 1A and fig. S1A) (*10*). After inducing TOMATO (TOM) expression by injecting tamoxifen (TAM), we used fluorescence-activated cell sorting (FACS) to enrich for $Gli1^{TOM+}$ keratinocytes of the TD ($SCA\text{-}1^+$) and HF bulge ($SCA\text{-}1^-$) and generated single-cell libraries (fig. S1B). Unsupervised clustering identified five distinct

[1]Black Family Stem Cell Institute, Department of Cell, Developmental, and Regenerative Biology, Icahn School of Medicine at Mount Sinai, New York, NY, USA. [2]Department of Genetics, Albert Einstein College of Medicine, New York, NY, USA. [3]Department of Neurology, and Neuroscience, Albert Einstein College of Medicine, New York, NY, USA. [4]Department of Biosciences and Nutrition, Karolinska Institutet, Huddinge, Sweden. [5]Department of Cell and Molecular Biology, Karolinska Institutet, Stockholm, Sweden.
*Corresponding author: elena.ezhkova@mssm.edu
†These authors contributed equally to this work.
‡Present address: Faculty of Fisheries Engineering, Kerala University of Fisheries and Ocean Studies, Kochi, Kerala, India.
§Present address: Center for Neuroscience, Department of Biotechnology, Cochin University of Science and Technology, Kerala, India.
¶Present address: GC Therapeutics Inc. Cambridge, MA, USA.

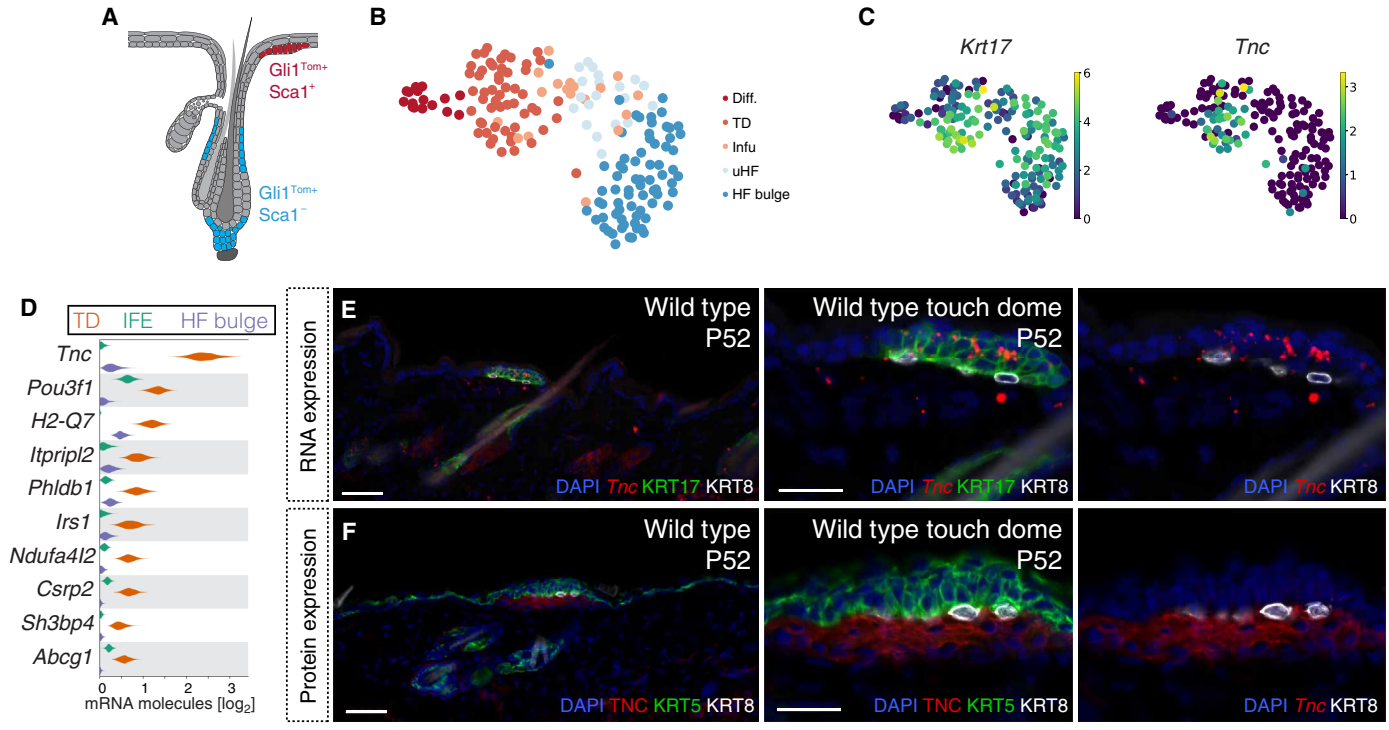

Fig. 1. *Tnc* is expressed in the TD keratinocytes of adult dorsal skin. (**A**) Schematic showing the Gli1^{TOM+} populations that were isolated for scRNA-seq. (**B**) Cell transcriptomes were visualized with Uniform Manifold Approximation and Projection (UMAP) and colored according to unsupervised (first-level) clustering. (**C**) Expression of *Krt17* and *Tnc* projected onto the UMAP. (**D**) Violin plot depicting the expression of TD signature genes in comparison to IFE basal and HF bulge cells. (**E**) Immunofluorescence (IF) of DAPI (blue), KRT17 (green), KRT8 (white), and in situ of *Tnc* RNA (red) in the TD of P52 wild-type mice. Note that *Tnc* RNA was detected in the TD keratinocytes, a subset of MCs and dermal cells below the TD. (**F**) IF of DAPI (blue), KRT5 (green), KRT8 (white), and TNC protein (red) in the TD of P52 wild-type mice. Note that TNC protein was detected only in the dermal cells below the TD. Scale bars, 50 μm for 20× and 25 μm for 40× images.

groups of epidermal cells, including a TD cluster marked by the expression of KRT17 (Fig. 1B and fig. S1, C and D) (*9*). Expression of dermal cell genes was absent from any identified clusters (fig. S1D). We identified that the KRT17 expressing TD cells also transcribed an extracellular matrix (ECM) protein encoding gene, *Tenascin-C* (*Tnc*) (Fig. 1C) (*11*, *12*). Upon further analysis to define the TD keratinocyte transcriptome, we compared it to the transcriptome of both IFE basal and HF bulge cells (see Materials and Methods) (*13*), which highlighted *Tnc* as the most highly expressed gene among TD-specific genes (Fig. 1D).

To confirm that *Tnc* mRNA is enriched in the TD keratinocytes in the adult epidermis, we performed in situ hybridization with a *Tnc*-specific probe in the dorsal skin of P52 mice. We observed that while *Tnc* mRNA was undetectable in the IFE of P52 dorsal skin, it was detected in the TD keratinocytes (Fig. 1E and fig. S1E). A subset of HF bulge/hair germ cells also expressed *Tnc* as previously described (Fig. 1D and fig. S1G) (*14*). We also observed *Tnc* expression in dermal cells that are located underneath the TD (Fig. 1E). As TNC is an ECM protein, we also inspected the expression pattern of the TNC protein. Immunofluorescence (IF) analysis of P52 dorsal skin revealed that TNC was detected in dermal cells underneath the TD and surrounding the HF bulge (Fig. 1F and fig. S1, F and H). Together, these analyses identified *Tnc* as a marker of the TD keratinocytes.

TD keratinocytes increase their proliferation during the anagen phase of the hair cycle

To further characterize the TD keratinocytes in the adult epidermis, we acquired *Tnc-CreER* mice (*15*) and crossed them with the (*ROSA*)*26Sor*$^{tm14(CAG-tdTomato)Hze}$/*J* (*R26*^{tdTomato}) reporter line to generate *Tnc-CreER; R26*^{tdTomato} animals which would express TOMATO protein exclusively in *Tnc* transcribing cells upon TAM injection. We injected *Tnc-CreER; R26*^{tdTomato} mice twice with TAM starting at P51 and collected dorsal skins at P60, P150, and P365 for IF analysis (Fig. 2A). Most of the KRT17^{+} TD cells (>98%) were labeled with TOMATO starting at P60 and remained labeled at all the following analyzed time points (Fig. 2, B to E). To confirm that *Tnc-CreER* does not label TD keratinocytes without TAM induction, we injected *Tnc-CreER; R26*^{tdTomato} mice twice with corn oil at P51 and collected dorsal skin at P60 (fig. S2A). We did not observe TOMATO expression (fig. S2A), confirming that *Tnc-CreER* is not leaky in the skin and labeling of TD keratinocytes is specific upon TAM induction. Together, these analyses show that *Tnc-CreER* is a robust tool to mark TD keratinocytes and that the labeling of TD cells persists even 1 year postlabeling. We also observed TOMATO expression in dermal cells and a few HF bulge cells (Fig. 2, B to D), consistent with our in situ hybridization data.

We next analyzed whether the TD keratinocytes proliferate in the adult dorsal skin to maintain themselves during homeostasis. As proliferation of many skin cells is linked to the hair cycle (*16*, *17*), we injected wild-type mice with 5-ethynyl-2'-deoxyuridine (EdU) at different phases of the hair cycle, namely, at P20 (telogen I), P27 (anagen), P41 (catagen), and P51 (telogen II), and then collected and analyzed skins 24 hours postinjection (Fig. 2F and fig. S2, B to F). Although we observed a few KRT17^{+} TD keratinocytes positive for EdU incorporation at P21, P42, and P52 (Fig. 2F and fig. S2, B, D, and E), there

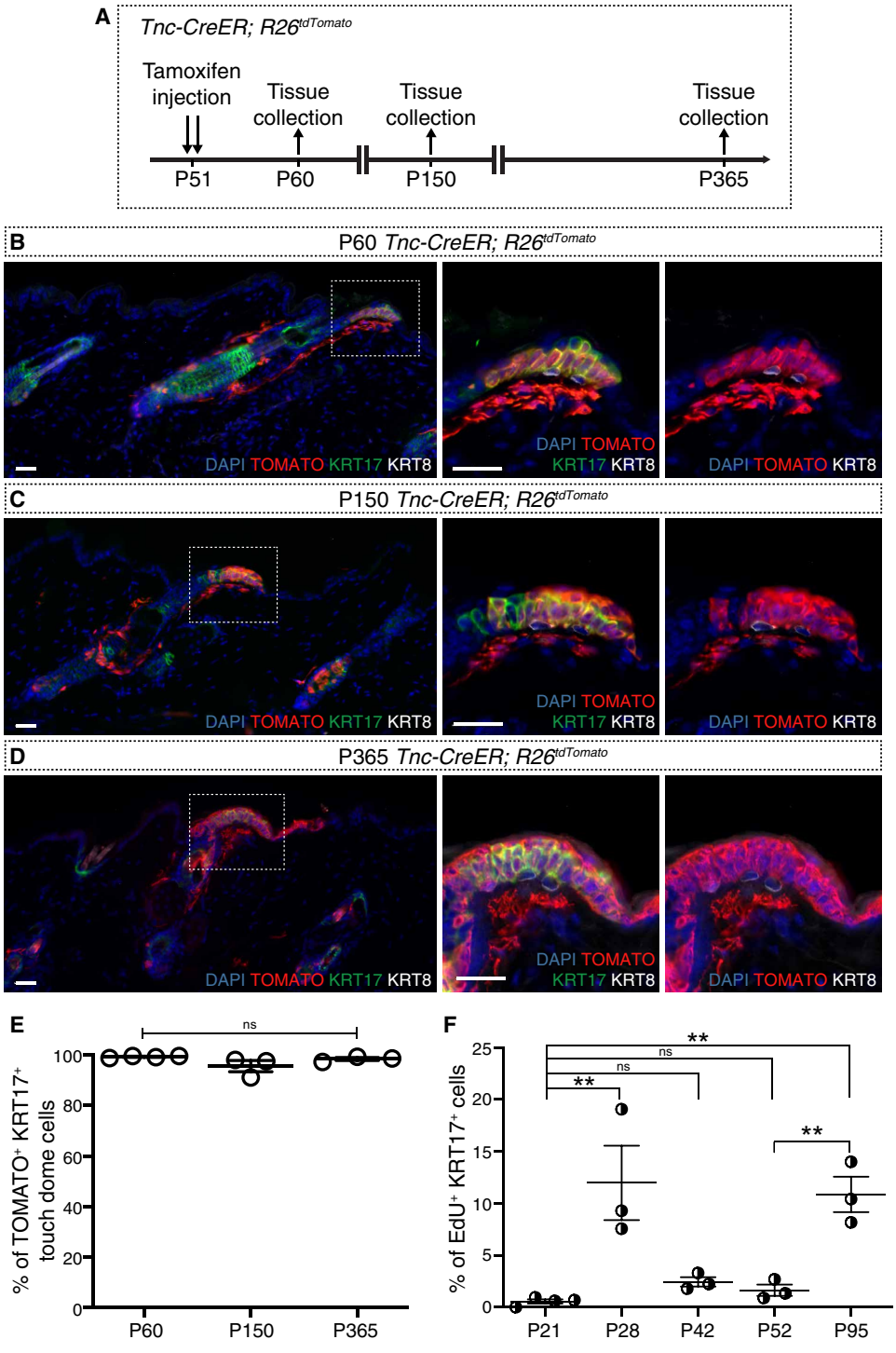

Fig. 2. *Tnc-CreER* efficiently labels TD keratinocytes. (**A**) Experimental design of lineage tracing in *Tnc-CreER; R26*^{tdTomato} mice. (**B** to **D**) *Tnc-CreER; R26*^{tdTomato} lineage tracing in the back skin of P60 (B), P150 (C), and P365 (D) mice, respectively. IF analysis of DAPI (blue) TOMATO (red), KRT17 (green), and KRT8 (white). Insets show a higher magnification of TOMATO expressing TD keratinocytes. (**E**) A scatterplot representing the average percentage ± SEM of TOMATO$^+$/ KRT17$^+$ cells in *Tnc-CreER; R26*^{tdTomato} back skin sections of P60, P150, and P365 mice (n = 100 TDs across three to four animals per time point). Nonparametric one-way ANOVA (Kruskal-Wallis test) was conducted. P value = 0.0619. (**F**) A scatterplot representing the average percentage ± SEM of EdU$^+$/KRT17$^+$ cells in the back skin of P21, P28, P42, P52, and P95 mice (n = 30 TDs across three to four animals per time point). One-way ANOVA (Dunnett's multiple comparisons test) was conducted. P values = 0.0014 (P21 versus P28); 0.83 (P21 versus P42); 0.97 (P21 versus P52); 0.0031 (P21 versus P95); 0.0099 (P52 versus P95). Scale bars, 25 μm.

was a significant increase in EdU$^+$ TD keratinocytes during the anagen phase at P28 (Fig. 2F and S2C). This suggests that the increase in proliferation of the TD keratinocytes might be coupled to the anagen phase of the hair cycle. To confirm this observation, we injected EdU during the subsequent anagen phase at P94 and observed that TD cells were indeed undergoing increased proliferation (Fig. 2F and fig. S2F). Together, these results establish that the TD keratinocytes are a proliferating, self-maintaining, specialized group of epidermal cells.

Tnc-expressing TD cells regenerate MCs upon mild injury

Previous studies have presented conflicting reports exploring whether MCs regenerate in adult animals (*9*, *18*–*22*). We thus asked whether TNC$^+$ TD keratinocytes contribute to MC regeneration after P50, when the mice have fully matured. We induced TOMATO expression in P51 *Tnc-CreER; R26^{tdTomato}* animals and collected skins at P60, P150, and P365, when the animals have undergone one or more hair cycles (fig. S3A). We observed that, while all TNC$^+$ TD keratinocytes were labeled with TOMATO at P60, around ~10% of KRT8$^+$ MCs were TOMATO$^+$ (fig. S3, B and E), which could be a consequence of low-level *Tnc* transcription in a subset of MCs. This is supported by the detection of *Tnc* RNA in MCs via in situ hybridization (Fig. 1E) and previous RNA sequencing (RNA-seq) studies reporting *Tnc* transcription in MCs (*23*). Furthermore, we observed a similar number of KRT8$^+$ and TOMATO$^+$ MCs at P150 (fig. S3, C and E). Although we noticed a modest increase in KRT8$^+$ and TOMATO$^+$ MCs at P365, this expansion was not significant when compared to P60 or P150 (fig. S3, D and E), indicating that MCs do not regenerate from TNC$^+$ TD keratinocytes after the animals fully mature.

It has also been shown that a superficial or mild injury to the adult skin leads to MC regeneration (*22*). However, the source of MC regeneration upon injury is unclear. Hence, to gain clarity on whether MCs themselves proliferate or arise from a progenitor population upon injury, we established a mild injury model where we waxed the back skin of P50 animals (fig. S3F). Next, we investigated whether MCs reduce in numbers following injury and whether they proliferate to recover their numbers. Therefore, we collected samples 24, 48, 72, and 96 hours postwax and conducted whole mount IF analysis of MC numbers and proliferation (Fig. 3A). We found that MC numbers reduced significantly, in comparison to unwaxed controls, 24 hours postinjury but recovered within 96 hours postinjury (Fig. 3, A and B). Analysis of a proliferative marker, Ki67, revealed that while surrounding epidermal cells underwent proliferation swiftly upon injury, we never detected proliferation of MCs (Fig. 3A). This led us to ask whether TD keratinocytes undergo proliferation to potentially contribute toward MC recovery postinjury. Analysis of Ki67 of KRT17$^+$ TD keratinocytes 24, 48, 72, and 96 hours postinjury revealed that contrary to our MC observations, TD keratinocytes started to significantly proliferate within 48 hours of waxing and continued to proliferate at time points where we saw the recovery of MC numbers (Fig. 3, C and D, and fig. S3G). Consequently, we examined whether TNC$^+$ TD keratinocytes are responsible for MC regeneration postinjury, we induced TOMATO expression at P51 and caused mild injury using waxing (Fig. 3E). The back skins were collected after one completed hair cycle and compared to uninjured controls (Fig. 3E). While control skin showed little to no MC regeneration, infliction of a mild injury resulted in a modest but significant increase in TOMATO$^+$ and KRT8$^+$ MCs after waxing (Fig. 3, F and G). To rule out whether inflicting an injury could drive *Tnc-CreER; R26^{tdTomato}*–mediated labeling of MCs without TAM induction, we waxed the back skin of *Tnc-CreER; R26^{tdTomato}* mice that were injected with corn oil and collected skin samples after the hair cycle was completed (fig. S3H). Although we observed very rare instances of TOMATO labeling of a single TD keratinocyte and a few dermal cells, we never observed TOMATO$^+$ and KRT8$^+$ MCs, confirming that the increase in TOMATO$^+$ and KRT8$^+$ MCs observed upon injury in TAM induced *Tnc-CreER* labeling is not a result of leaky *Cre* activity (fig. S3, I and J). Together, these analyses led us to conclude that, while TNC$^+$ TD cells do not give rise to MCs during homeostasis, they are capable of regenerating MCs upon injury.

Tnc is dispensable for TD and MC maintenance

We next asked whether TNC has a functional role in maintaining the TD and MCs in the adult dorsal skin. Therefore, we analyzed the number of TD keratinocytes and MCs in the dorsal skin of *Tnc*$^{-/-}$ [*Tnc* knockout (KO)] mutant mice. We first confirmed that TNC is lost in *Tnc* KO mice by performing IF analysis of the dorsal skin of P75 mice (fig. S4A). Curiously, we found that ablation of *Tnc* does not affect the number of KRT17$^+$ TD cells (fig. S4, B and C), nor does it affect the number of KRT8$^+$ MCs (fig. S4, D and E). Considering that TNC is an ECM protein that is secreted into the TD-associated stromal cells, it could play a role in regulating the function of MCs by controlling their innervation. Therefore, we stained for NF200, a marker for slowly adapting type I (SAI) neurons that innervate mature MCs in the adult skin and found that loss of *Tnc* does not alter SAI innervation of MCs (fig. S4F) (*4*, *24*). Together, these results suggest that TNC itself does not have a functional role in TD cell or MC maintenance and is not required to maintain innervation during homeostasis.

TNC$^+$ TD keratinocytes are very similar to the IFE

Given that the *Tnc-CreER* robustly labels the TD keratinocytes, we used FACS to isolate these cells for transcriptional and chromatin analyses and comparison with other epidermal compartments of the skin. TD keratinocytes were gated as Ep-CAM$^+$, α6 integrin$^+$, SCA-1$^+$, and TOMATO$^+$ cells. IFE and HF keratinocyte populations were gated as Ep-CAM$^+$, α6 integrin$^+$, SCA-1$^+$, TOMATO$^-$ and Ep-CAM$^+$, α6 integrin$^+$, SCA-1$^-$, TOMATO$^-$, respectively (fig. S5A). We confirmed the accuracy of the gating strategy by performing quantitative reverse transcription polymerase chain reaction (qRT-PCR) for TD-, IFE-, and HF-specific genes in the isolated populations (fig. S5B). Following isolation, we performed bulk RNA-seq on all three populations. Clustering analysis revealed that the transcriptional profile of the TD population is highly similar to that of the IFE with only 229 genes differentially up-regulated in TD (Fig. 4, A and B, and table S1). There were only 54 uniquely enriched genes in the TD keratinocytes (Fig. 4B and table S2), and gene ontology analysis revealed that the TD unique genes are involved in regulatory processes such as axon guidance (*Meg3* and *Slit1*) (*25*, *26*), innervation (*Edn1* and *Nptx1*) (*27*, *28*), and sensory perception of pain (*Aqp1* and *Penk*) (*29*, *30*) that are essential for proper MC function (Fig. 4C).

Next, we performed assay for transposase-accessible chromatin with sequencing (ATAC-seq) to access the global chromatin landscape of the IFE, HF, and TD populations. Again, similar to transcriptional studies, the open chromatin landscapes between IFE and the TD cells are remarkably similar (Fig. 4D). Together, these genomic studies revealed that, although during homeostasis, the TD is an autonomous compartment in the epidermis, its transcriptional and chromatin landscape is very similar to that of the IFE. This finding led us to investigate whether the TD cells have the capacity to take on an IFE fate. Our

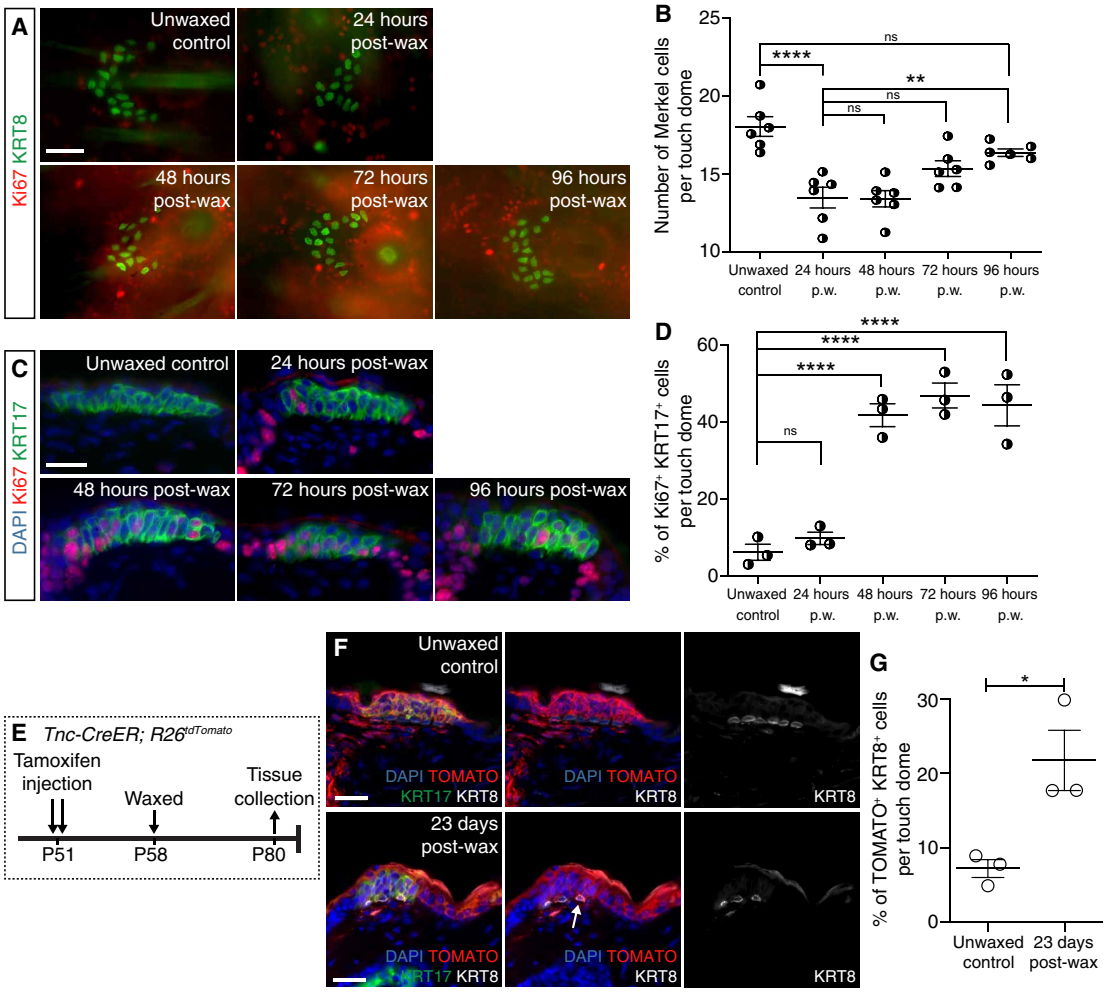

Fig. 3. TNC expressing TD cells give rise to MCs upon mild injury. (**A**) Whole-mount IF analysis of KRT8 (green) and Ki67 (red) in TDs of dorsal skin of unwaxed control, 24-, 48-, 72-, and 96-hour post-wax (p.w.) mice. (**B**) A scatterplot representing the average number of KRT8$^+$ MCs in TDs of dorsal skin of unwaxed control, 24-, 48-, 72-, and 96-hours p.w. mice (n = 30 to 40 TDs across six animals per time point). One-way ANOVA (Dunnett's multiple comparisons test) was conducted. P values = <0.0001 (unwaxed control versus 24 hours p.w.); 0.11 (unwaxed control versus 96 hours p.w.); >0.99 (24 hours p.w. versus 48 hours p.w.); 0.06 (24 hours p.w. versus 72 hours p.w.); 0.0028 (24 hours p.w. versus 96 hours p.w.). (**C**) IF analysis of DAPI (blue), KRT17 (green), and Ki67 (red) in the dorsal skin of unwaxed control, 24-, 48-, 72-, and 96-hours p.w. mice. (**D**) A scatterplot representing the average percentage ± SEM of Ki67$^+$/KRT17$^+$ cells in TDs of dorsal skin of unwaxed control, 24-, 48-, 72-, and 96-hours p.w. mice (n = 15 to 20 TDs across three animals per time point). One-way ANOVA (Dunnett's multiple comparisons test) was conducted. P values = 0.085 (unwaxed control versus 24 hours p.w.); <0.0001 (unwaxed control versus 48 hours p.w.); <0.0001 (unwaxed control versus 72 hours p.w.); <0.0001 (unwaxed control versus 96 hours p.w.). (**E**) Experimental design of lineage tracing in *Tnc-CreER; R26^{tdTomato}* mice. The dorsal skin was waxed at P58 and collected 23 days later. (**F**) IF analysis of DAPI (blue), TOMATO (red), KRT17 (green), and KRT8 (white) in P80 unwaxed control and waxed skin of *Tnc-CreER; R26^{tdTomato}* mice. (**G**) A scatterplot representing the average percentage ± SEM of TOMATO$^+$/KRT8$^+$ cells in unwaxed and 23 days p.w. *Tnc-CreER; R26^{tdTomato}* mice (n = 30 TDs per group across three animals). An unpaired t test was conducted to test for significance. P value = 0.0262. Scale bars, 25 μm.

long-term lineage tracing experiments with *Tnc-CreER; R26^{tdTomato}* (Fig. 4, E to H) revealed that, at P365, 80% of TOMATO$^+$ TDs had KRT5$^+$ KRT17$^-$ TOMATO$^+$ IFE cells located adjacent to the TD (Fig. 4, H and I). Together, these data show that the TD keratinocytes are primed to take on an IFE fate.

TNC$^+$ TD keratinocytes share molecular characteristics with HF keratinocytes

Although global transcriptional and chromatin analyses revealed that the TD is highly similar to the IFE, previous studies have shown that the TD cells express several HF markers such as KRT17, GLI1, and CD200 (*9*, *10*, *21*, *31*). We further analyzed our genomic data to investigate whether the TD and HF populations share more molecular characteristics. Of the 229 genes that are differentially up-regulated in the TD when compared to the IFE, 175 genes were HF-associated genes, such as *Krt17* and *Gli1*, and intriguingly HFSC genes *Cd34*, *Lgr5*, *Fgf18*, and *Lhx2* (Figs. 4B and 5A and table S3) (*32*–*35*). We confirmed that these genes are transcribed in both HF and TD but not in the IFE via qRT-PCR (Fig. 5B) and IF analysis (Fig. 5C and fig. S5C).

Previously published lineage tracing experiments using *Cre* drivers under the promoter of HF- and TD-expressed genes, such as KRT17 and GLI1, showed colabeling of TD and HF cell populations (*9*, *10*, *21*). To delineate whether HF lineages contribute

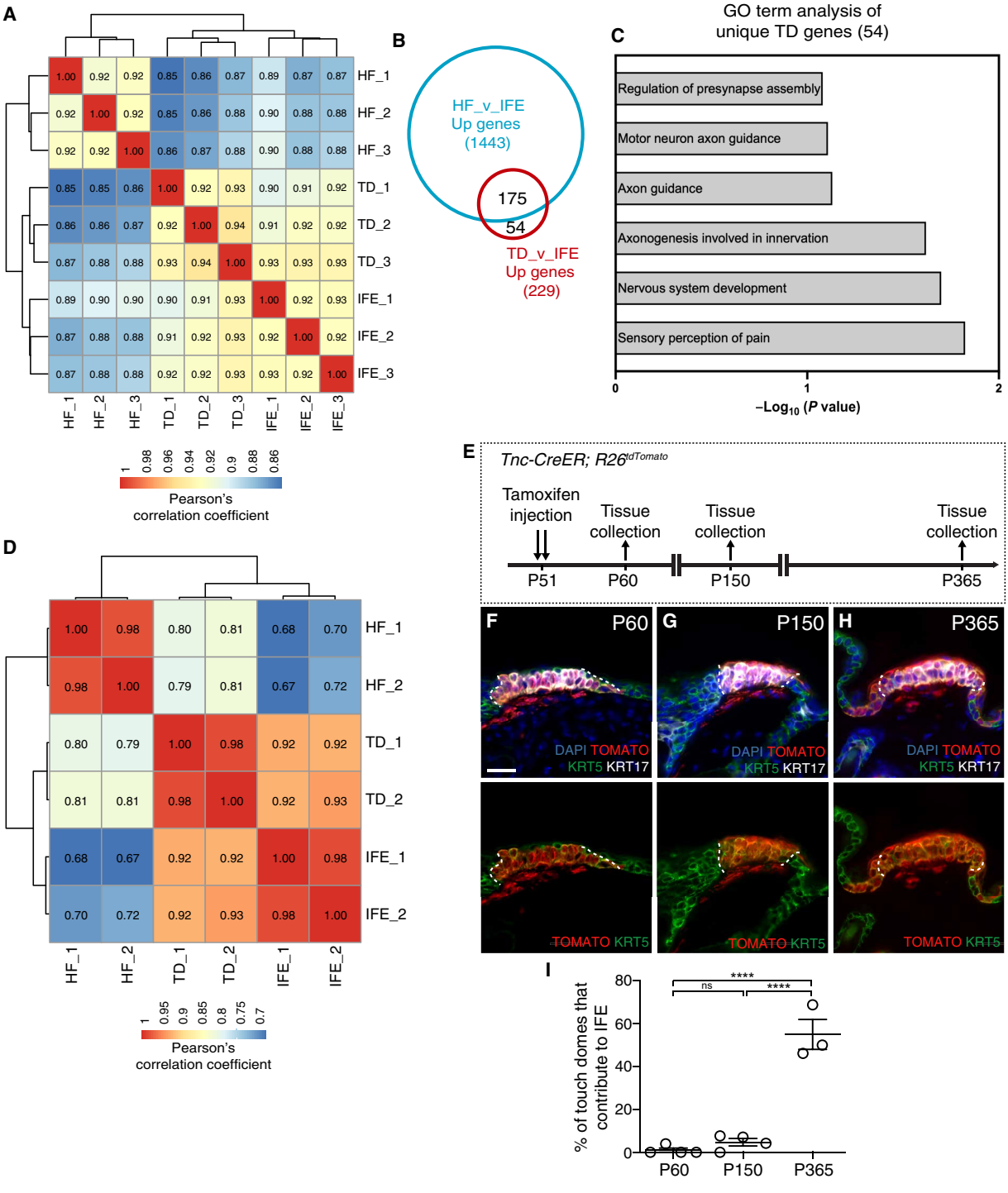

Fig. 4. TD keratinocytes are similar to the IFE keratinocytes. (**A**) Heatmap showing the correlation and clustering of the FACS-isolated IFE, TD, and HF cells from the dorsal skin of P60 *Tnc-CreER; R26*^{tdTomato} mice, based on the log-transformed read counts of all genes in RNA-seq data. RNA-seq analysis was done on three biological replicates for each group from at least two independent litters. (**B**) Venn diagram depicting that 175 of the 229 genes significantly up-regulated in TD when compared to IFE were also expressed more highly in HF cells. (**C**) Gene Ontology (GO) analysis of the 54 TD unique genes. (**D**) Heatmap showing the correlation and clustering of open chromatin in FACS-isolated IFE, TD, and HF cells from the dorsal skin of P60 *Tnc-CreER; R26*^{tdTomato} mice based on the log-transformed read counts at all ATAC-seq peaks. The numbers are Pearson's correlation coefficients. ATAC-seq analysis was done on two biological replicates for each group from at least two independent litters. (**E**) Experimental design of long-term lineage tracing in *Tnc-CreER; R26*^{tdTomato} mice starting at P51. The dorsal skin was collected at P150 and P365. (**F** to **H**) IF analysis of DAPI (blue), TOMATO (red), KRT17 (white), and KRT5 (green) in the dorsal skin of P60 (F), P150 (G), and P365 (H) mice. White dashed lines indicate the border of KRT17$^+$ TD cells. (**I**) A scatterplot representing the average percentage ± SEM of TOMATO$^+$ TDs that have contributed to the nearby IFE ($n = 60$ TDs for each time point across three to four animals). One-way ANOVA (Dunnett's multiple comparisons test) was conducted. *P* values = 0.65 (P60 versus P150); <0.0001 (P60 versus P365); <0.0001 (P150 versus P365). Scale bars, 25 μm.

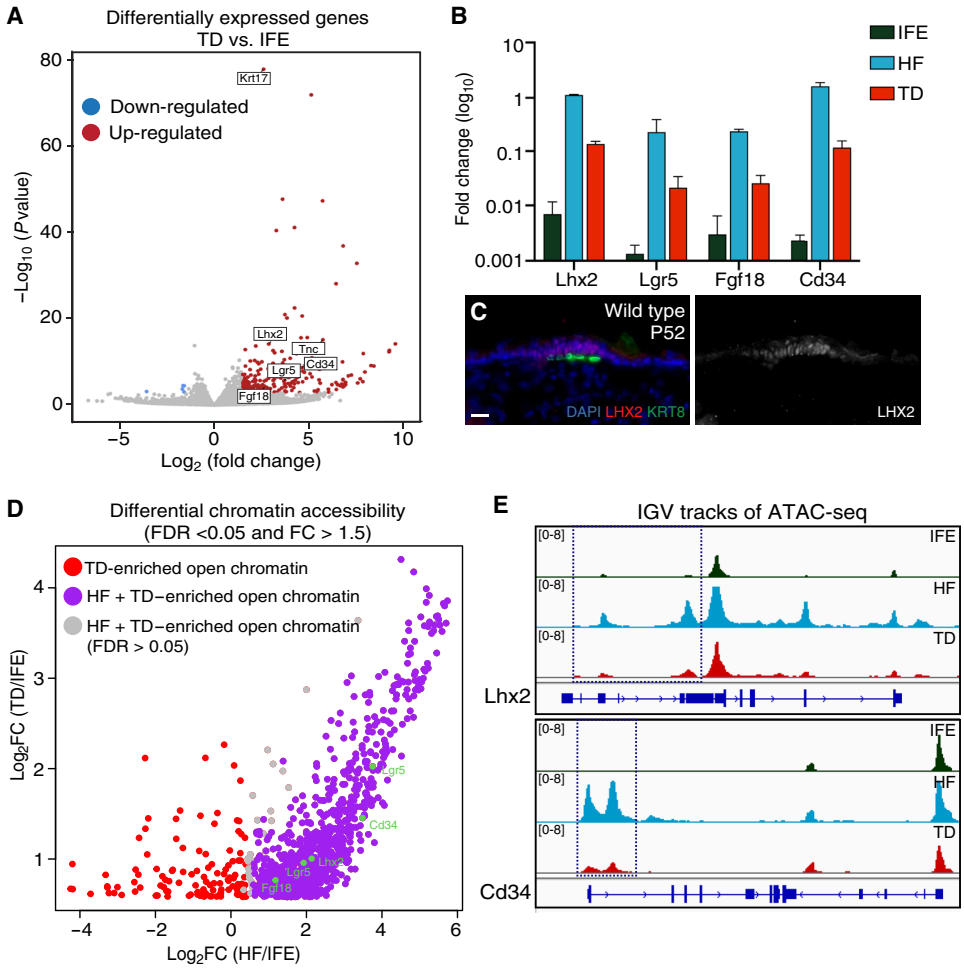

Fig. 5. TD keratinocytes share molecular characteristics with the HF. (**A**) Volcano plot depicting the differentially expressed genes in FACS-purified TD versus IFE cells from the dorsal skin of P60 *Tnc-CreER; R26*^{tdTomato} mice. Genes with absolute fold change > 1.5 and adjusted *P* value < 0.05 were considered significantly up-regulated or down-regulated in TD cells. (**B**) RT-qPCR analysis of HF genes that were identified to be expressed higher in TD cells than in IFE via RNA-seq and which have greater chromatin accessibility in HF and TD than in the IFE. (**C**) IF analysis of DAPI (blue) and HFSC marker LHX2 (red) in TD which was identified by the presence of KRT8 (green) expressing MCs. LHX2 single channel is shown in gray. Scale bar, 10 μm. (**D**) Scatterplot comparing the degrees of chromatin accessibility changes in TD and HF versus IFE, revealing that of 1021 ATAC-seq peaks that are significantly more accessible [false discovery rate (FDR) < 0.05 and fold change (FC) >1.5] in the TD than in the IFE, 881 of them are also significantly greater in HF, including peaks at some key HF genes (green dots). (**E**) IGV tracks of ATAC-seq profiles at selected HF signature genes in FACS-isolated IFE, HF, and TD keratinocytes.

toward TD homeostasis after a longer tracing period, we used *Sox9-CreER; R26*$^{mT/mG}$ animals generated by crossing *Sox9-CreER* (*36*) mice to the *(ROSA)26Sor*$^{tm4(ACTB-tdTomato,-EGFP)Luo}$*/J* (*R26*$^{mT/mG}$) reporter line. In *Sox9-CreER; R26*$^{mT/mG}$ mice, application of TAM at P51 for three consecutive days leads to efficient labeling of all populations of the HFs but not the TD (fig. S5, D and E). We then collected the skins of these mice at P150 and observed that while the entire HF remained green fluorescent protein positive (GFP$^+$), as expected, we did not detect any GFP$^+$ cells in the TD (fig. S5E). Therefore, although the TD keratinocytes express several genes associated with the HF, the HF itself is not responsible for the maintenance of these cells. Investigation of chromatin accessibility revealed that of 1021 ATAC peaks that are significantly more accessible in the TD when compared to the IFE, 881 of them are also HF enriched (Fig. 5D). This suggests that open chromatin regions in TD that are distinct from the IFE are also significantly more accessible in the HF. Integrative Genomics Viewer (IGV) tracks of ATAC-seq profiles show that key HFSC genes *Lhx2* and *Cd34* contain very similar high open chromatin regions (i.e., peaks; at nonpromoters) in the HF and TD that are not accessible in the IFE (Fig. 5E). Overall, these analyses have identified that, while the global transcriptional and chromatin landscapes of the TD keratinocytes are very similar to those of the IFE keratinocytes, the critical differences between these populations lie in the fact that the TD also shares HF-associated transcriptional and chromatin characteristics.

DISCUSSION

In this study, the scRNA-seq transcriptomic analysis identified *Tnc*, an ECM protein coding gene, to be highly enriched in the TD keratinocytes. Lineage-tracing experiments showed that the *Tnc-CreER* mouse line is a robust tool for marking and isolating TD keratinocytes. *Tnc-CreER/Tomato*–traced cells persist in the TD even after

1 year postlabeling, and TD keratinocytes increase their proliferation rates to self-renew during the anagen phase of the hair cycle, showing that the TD maintains itself as an autonomous epidermal compartment in the adult skin. We did not observe that TNC-expressing TD cells give rise to MCs in the homeostatic skin. Notably, we observed that MC numbers significantly reduce upon mild injury but recover within 72 hours. This recovery cannot be attributed to MC proliferation. However, TD keratinocytes start to proliferate within 48 hours of injury and continue to proliferate during MC recovery. Lineage tracing analysis revealed an increase in TOMATO-labeled MCs, indicating that TD keratinocytes are potential progenitors during MC regeneration. RNA-seq and ATAC-seq analyses revealed that the transcriptional and chromatin landscape of the TD keratinocytes is remarkably similar to that of the IFE keratinocytes, and these cells can acquire an IFE cell fate over time in the homeostatic adult skin. Notably, our RNA- and ATAC-seq analyses also revealed that the TD keratinocytes share certain molecular signatures with the HF cells. Particularly, the TD keratinocytes not only express key HFSC genes but the open chromatin landscape of the TD keratinocytes that differs from the IFE is enriched for the HF lineage. This highlights the fact that the TD keratinocytes in the adult skin have unique molecular characteristics that are distinct from the IFE and HF lineages.

Several genes, such as *Gli1* and *Krt17*, have been shown to be expressed in TD keratinocytes (*9*, *10*). However, these genes are also abundantly expressed in HFs (*9*, *10*, *37*). Through scRNA-seq studies, we uncovered that the *Tnc* gene is predominantly expressed in TD keratinocytes, compared to HF or IFE. Our lineage tracing experiments further substantiated that TNC-expressing cells are notably more prevalent in TD than other skin epithelial cells. Intriguingly, when analyzing *Tnc* KO mice, we found that TNC is not required for either MC or TD maintenance or innervation, hinting at the potential compensatory roles of other ECM proteins in TD homeostasis. Future studies will delve into the role of TNC in TD regeneration after injury, TD maintenance during aging, and the possible involvement of TD cells in carcinogenesis, including MC carcinoma (*38*).

Numerous studies in adult mouse skin have illustrated the presence of spatially distinct domains in the IFE that express specific markers and proliferate at different rates (*13*, *39*–*42*). These domains rarely expand out but rather are maintained by local epidermal stem cells (EpSCs) (*39*, *41*, *43*). The TD keratinocyte cluster seems to be functioning similarly, evident by the observation that labeled TD keratinocytes maintain their precise boundaries months postlabeling. Moreover, its proliferative activity is distinct from its neighboring IFE keratinocytes; rather, it is coupled to the hair cycle. Although we do not have direct evidence of the factors that bestow this specificity of the TD keratinocytes, one can speculate that external cues, such as Shh signaling from the innervating sensory neurons, might be providing the environment for this specialized behavior (*44*).

Studies of the adult murine skin have shown that each epithelial compartment is maintained by a specialized population of stem cells, such as EpSCs that maintain the epidermis and HFSCs that maintain HFs (*16*). While EpSCs are unipotent and only give rise to the epidermis, HFSCs can also give rise to the epidermis upon wounding (*45*, *46*). During normal homeostasis, TD cells replenish and maintain themselves. However, external signaling can induce TD cells to give rise to de novo HFs (*10*), and isolated TD cells can give rise to IFE cells in skin grafts (*47*). In addition, our study uncovered the capacity of TD cells to give rise to MCs and IFE cells upon injury or aging, respectively, thereby highlighting that the TD cells are a unique population of cells in the epidermis that has the potential to give rise to MC, IFE, and HF lineages. The analysis of the chromatin and transcriptional landscape of the TD keratinocytes showed that they are very similar to those of the IFE, yet they express several HF genes and exhibit HF-enriched chromatin accessibility but at a lower level than what we observed in the HF keratinocytes. We speculate that this unique chromatin characteristic of the TD keratinocytes is what allows them to take on an IFE or HF lineage fate. Overall, our molecular characterization of the TD bridges the gap in our understanding of how these specialized epidermal cells are capable of committing to several skin epithelial lineages.

Given that all lineage tracing experiments in the TD have used *Cre* drivers under the promoter of HF genes, such as *Krt17* and *Gli1*, as well as the transgenic line used in this study, which all colabel the TD keratinocytes and HF cell populations (*9*, *10*), it has been challenging to parse the contribution of the HF to the TD during homeostasis. By conducting long-term lineage tracing with the *Sox9-CreER* transgenic line that robustly labels all HF cell populations (*36*) but not the TD, we unequivocally show that the HF does not contribute to TD keratinocyte maintenance in the adult skin. Together, our work has uncovered that—although TD cells express several HF lineage genes and during development come from HF cells (*7*)—the TD is an autonomous epidermal compartment that functions independently of the IFE and HF to maintain itself in the adult homeostatic skin.

During development, MCs originate from embryonic epidermal progenitors, specifically from the inside of the developing HFs (*7*). However, MC turnover and regeneration in the adult mouse skin have remained a point of contention for many years. While some lineage tracing studies report that MC numbers vary during the hair cycle and they are regularly replaced postnatally (*9*, *18*–*21*), others conclude that MCs are long-lived with little to no turnover rate in the adult skin (*22*). Our lineage tracing studies with *Tnc-CreER; R26*^{tdTomato} animals were exclusively performed after animals reached full maturity, and we did not observe that TNC-expressing TD keratinocytes give rise to MCs. Although the infliction of a mild injury results in a decrease in MCs, we did not detect any proliferation in the MCs. However, mild injury–induced TD keratinocyte proliferation and lineage tracing confirmed TD keratinocytes as MC progenitors in the adult skin. It is of note that lineage tracing studies reporting MC turnover were induced in young adult mice before reaching maturity at P50 (*21*). The epidermis undergoes many changes to adapt to the growing size of the organism until P50 (*48*). Therefore, the discrepancies between MC regeneration pre- and post-P50 lineage tracing studies could be attributed to the fact that epidermal compartments behave differently during these stages of adulthood. Further investigation regarding TD and MC dynamics in the epidermis of young adults versus fully mature animals will allow us to tease apart these differences.

One of the major challenges of regenerative medicine is the induction of complex epithelial structures from a singular source of progenitors. Our study demonstrates that the TD keratinocytes encompass unique EpSCs that exhibit characteristics of other epidermal lineages and therefore can

potentially be manipulated to establish a complex epithelial structure composed of all epidermal appendages. Age-dependent loss of MCs has been linked to alloknesis, a condition where light touch invokes itch (*49*–*51*). Therefore, harnessing the TD's potential to regenerate MCs could be beneficial for alleviating chronic itch. Furthermore, cutaneous carcinomas such as basal cell carcinoma have been shown to originate from epidermal lineages including the TD (*10*, *52*), and MC carcinoma has been speculated to arise from MC progenitors in the adult skin (*53*, *54*). Therefore, dissecting the dynamics, function, and molecular characteristics of these specialized epidermal cells not only has implications in cancer therapeutics and regenerative medicine but also will aid in our understanding of adult tissue biology.

MATERIALS AND METHODS

Mice

Mice were housed in the Center for Comparative Medicine and Surgery at Icahn School of Medicine at Mount Sinai (ISMMS) in accordance with the Institutional Animal Care and Use Committee with approved protocol LA11-0020 or at the Preclinical Laboratory Animal Facility at Karolinska University Hospital in Huddinge, Sweden, in accordance with Swedish legislation and approved by the Linköping Animal Ethics Committees. *Tnc-CreER* mice were gifted by C.M. Hao and A.B. Fogo (*15*), *Gli-CreER*^{T2} were received from F. Aberger (*55*), *Sox9-CreER* mice were gifted by T. Chen (*36*), and *Tnc*$^{-/-}$ KO mice were gifted by B.G. Sharifi. (*ROSA*)*26Sor*$^{tm4(ACTB-tdTomato,-EGFP)Luo}$*/J* (stock number: 007676) and (*ROSA*)*26Sor*$^{tm14(CAG-tdTomato)Hze}$*/J* (stock number: 007914) mice were obtained from The Jackson Laboratory. Mice were genotyped by PCR using DNA extracted from ear skin. Three animals from at least two independent litters were used for each analysis, except for scRNA-seq studies wherein a total of four animals were processed on two different days.

Lineage tracing experiments

To induce TOMATO expression in *Tnc-CreER; R26*^{tdTomato} mice, animals were injected intraperitoneally with 100 μg/g body weight of TAM (20 mg/ml dissolved in corn oil) (Sigma-Aldrich, St. Louis, MO) daily for two consecutive days starting at P51 and then collected at desired time points as indicated in the figures. To detect leaky *Cre* activity *Tnc-CreER; R26*^{tdTomato} mice, animals were injected intraperitoneally with 100 μl of corn oil daily for two consecutive days starting at P51 and then collected at desired time points as indicated in the figures. For inducing GFP expression in *Sox9-CreER; R26*$^{mT/mG}$ mice, animals were injected intraperitoneally with 100 μg/g body weight of TAM daily for three consecutive days starting at P51 and then collected at desired time points as indicated in the figures. To cause mild injury, *Tnc-CreER; R26*^{tdTomato} mice were either waxed once 6 days post-induction.

IF, in situ hybridization, and microscopy

For IF staining, tissues were collected and embedded into optimal cutting temperature (OCT) compound blocks (Tissue-Tek, Torrance, CA) and subsequently cut into 10-μm sections using a Leica Cryostat. Slides were fixed for 10 min in 4% paraformaldehyde (PFA; Electron Microscopy Sciences) in phosphate-buffered saline (PBS) and blocked for 1 hour at room temperature or overnight at 4°C in PBS with blocking solution [1% Triton X-100, 1% bovine serum albumin (BSA), and 0.25% normal donkey serum]. Primary antibodies were diluted in blocking solution, and incubations were carried out for 1 hour at room temperature or overnight at 4°C, followed by incubation in secondary antibodies for 1 hour at room temperature. Slides were counterstained with 4′,6-diamidino-2-phenylindole (DAPI) and mounted using antifade mounting media. In situ hybridization for *Tnc was* performed using RNAscope probes and a 2.5HD-RED detection kit (Advanced Cell Diagnostics), according to the manufacturer's protocol.

For whole-mount IF staining, back skins were collected and fixed in 4% PFA for 3 hours at room temperature and followed up with four washes with 1× PBS. Skins were blocked overnight in blocking solution. Primary antibodies diluted in blocking solution were incubated for 72 hours at room temperature, followed by incubation in secondary antibodies for 48 hours at room temperature. Skins were counterstained with DAPI followed by tissue clearing protocol using benzyl alcohol/benzyl benzoate (BA/BB). Skins were dehydrated by methanol followed by tissue clearing by 1:2 BA/BB and mounted on slides. Skin sections or whole-mount tissues were imaged using a Leica DM5500 upright slide microscope using 10×, 20×, or 40× objectives.

Antibodies

The following primary antibodies were used: KRT8 (Developmental Studies Hybridoma Bank, TROMA-1, 1:500), KRT17 (Abcam, ab109725, 1:500), KRT5 (BioLegend, 905901, 1:500), TNC (Sigma-Aldrich, AB19011, 1:250), GFP (Abcam, ab13970, 1:1000), SOX9 (Abcam, ab185966, 1:500), TOMATO (OriGene, AB8181-200, 1:500), NF200 (Abcam, ab8135, 1:500), LHX2 (Abcam, ab184337, 1:500), and Ki67 (Abcam, ab15580, 1:500). For IF staining, secondary antibodies were coupled with Alexa Fluor 488, 549, or 649 from Jackson ImmunoResearch (1:1000).

EdU pulse-chase experiment

Mice were injected with 125 μg of EdU in solution (*40*). Skin samples were collected 2 hours after injection and embedded in OCT. Slides were cut into sections using a Leica Cryostat and stored at −80°C until use. Slides were fixed in 4% PFA and permeabilized using 0.5% Triton X-100, followed by washes with 3% BSA and a 30-min incubation with a Click-iT reaction cocktail (Thermo Fisher Scientific, C10337). Slides were washed twice before proceeding with IF staining as described above.

Quantification and statistics

Quantification of MCs per TD or TD cells was performed by manually counting all positively stained and costained cells from each section examined. The mean proportion of costained cells for each animal was calculated and used in statistical analysis. Statistical calculations were performed using GraphPad Prism software. To determine the significance between the two groups, an unpaired *t* test was used. Nonparametric one-way analysis of variance (ANOVA; Kruskal-Wallis test) or ordinary one-way ANOVA (Dunnett's multiple comparisons test) was conducted to compare means between several experimental groups or against a single control group, respectively. For all statistical tests, $P < 0.05$ was considered for statistical significance, and the actual *P* values (to four decimal places) are provided in the figure legends. Significance levels were defined as $*P < 0.05$, $**P < 0.001$, $***P < 0.001$, $****P < 0.0001$, and ns (not significant). The number of biological replicates for each sample group is indicated in figure legends.

FACS for bulk RNA- and ATAC-seq experiments

Basal epidermis and HF cells were isolated and pooled from multiple P60 *Tnc-CreER R26*^{tdTomato} mice which were TAM-injected two times at P51 and 52 by FACS. Briefly, P60 *Tnc-CreER; R26*^{tdTomato} back skins were separated from the back of mice, scrapped of fat at dermis side, and incubated for 1 hour in 0.25% trypsin with 1 mM EDTA (Corning Cellgro, Manassas, Virginia, USA). Epidermal and HF cells were scraped off the back skin, passed through a 40-μm cell strainer, and collected.

The cell suspension was stained in Hanks' balanced salt solution (HBSS) + 2% fetal bovine serum with 1:100 SCA1-Cy7 (BioLegend), 1:100 α6 integrin–fluorescein isothiocyanate (BioLegend), and 1:500 Ep-CAM–Allophycocyanin) (BioLegend) for 30 min on ice and washed twice with 1× HBSS before cell sorting in HBSS with DAPI. TD cells were sorted as Ep-CAM$^+$, SCA-1$^+$, α6 integrin$^+$, and TOMATO$^+$. IFE cells were sorted as Ep-CAM$^+$, α6 integrin$^+$, SCA-1$^+$, and TOMATO$^-$. HF cells were sorted as Ep-CAM$^+$, α6 integrin$^+$, SCA-1$^-$, and TOMATO$^-$. All cell isolations were performed on a FACS IMI5L instrument (BD Biosciences) in the Flow Cytometry Core Facility at the Icahn School of Medicine at Mount Sinai.

RNA purification, RT-qPCR, and RNA-seq library preparation

A total of 50,000 FACS-purified cells were collected directly into the RLT Plus buffer (QIAGEN), and RNA was purified from these sorted cells with the RNeasy Plus Micro Kit (QIAGEN) according to the manufacturer's instructions. To perform RT-qPCR, cDNA was reverse-transcribed from 50 ng of total RNA using qScript cDNA SuperMix (Quanta Biosciences, Gaithersburg, Maryland, USA). Results were normalized to *GAPDH* mRNA levels. Primer sequences are available below (Table 1). Before library construction, sample quality was measured using an Agilent Bioanalyzer. Only samples with RNA integrity numbers of >8 were used for library preparation.

For generating RNA-seq libraries, 50 ng of total RNA was subjected to polyadenylate selection using Universal Plus mRNA-Seq with NuQuant (TECAN). Following elution, mRNA was subjected to fragmentation at 94°C for 8 min. First strand, second-strand cDNA synthesis, end repair, adapter ligation, and amplification were carried out using Universal Plus mRNA-Seq with NuQuant (TECAN) and by following the manufacturer's instructions.

scRNA-seq experiments and data analysis

Gli1-Cre^{ERT2}*; Rosa26*^{tdTomato} mice aged 7 weeks (second telogen) were treated twice with 3 mg of TAM intraperitoneally in corn oil (20 mg/ml) with 1 day in between the two injections. Seven days later, epidermal cells were isolated as described previously (*33*). Briefly, clipped and disinfected dorsal skin was isolated, dermal and adipose tissue was removed, and strips of skin were floated on trypsin for 2 hours at 32°C. Epidermal tissue was subsequently scraped into Minimum Essential Medium Eagle-Spinner modification (S-MEM) media/1% BSA, and single cells were isolated by magnetic stirring at

Table 1. List of primers for qPCR validation. Fw, forward; Rv, reverse.

Krt10 Fw	AACTCTACTGGGAGTTCAGG
Krt10 Rv	GATTTTCTTGAGGACCCCAC
Gli1 Fw	GTCAGGGTCCCAGGGTTATG
Gli1 Rv	GAGAGCCCGCTTCTTTGTTA
Pou3f1 Fw	AGTTCGCCAAGCAGTTCAAG
Pou3f1 Rv	TGGTCTGCGAGAACACGTTA
KRT10 Fw	GGAGGGTAAAATCAAGGAGTGGTA
KRT10 Rv	TCAATCTGCAGCAGCACGTT
Ascl2 Fw	GGAGCTGCTTGACTTTTCCA
Ascl2 Rv	GTAAGGCATAGGCCCAGGTT
GAPDH Fw	GTGAAGGTCGGTGTGAACG
GAPDH Rv	TCTCCATGGTGGTGAAGACA
PPIB Fw	GTGAGCGCTTCCCAGATGAGA
PPIB Rv	TGCCGGAGTCGACAATGATG
CD34 Fw	CAAGTTGTGGTGGGAAGAA
CD34 Rv	GAGGCGAGAGAGGAGAAA
Lhx2 Fw	CTGGGTCTTCCCTACTACAA
Lhx2 Rv	TTCAGCATCGTTCTCGTTAC
Fgf18 Fw	CCAAGTACTCTGGTTGGTATG
Fgf18 Rv	GTGTACATCTTGCTGGTTCT
NFATc1 Fw	GGTGCCTTTTGCGAGCAGTATC
NFATc1 Rv	CGTATGGACCAGAATGTGACGG
FOXc1 Fw	GCAGAACAGCATACGGCACAAC
FOXc1 Rv	AGGAAGCTGCCGTTCTCGAACA

120 rpm for 20 min at room temperature. The resulting cell suspension was filtered through 70- and 40-μm cell strainers and resuspended in Defined Keratinocyte Serum-free Medium without supplement (DK-SFM; Gibco, #10744019). Cells were stained for FACS with SCA-1 (rat monoclonal anti–SCA-1; BD Biosciences, catalog no. 561021) and CD34 (rat monoclonal anti-CD34; Thermo Fisher Scientific, catalog no. 14-0341-85; RRID: AB_467211) antibodies for 1 hour on ice, sorted into Poly(hydroxyethyl methacrylate)–coated tubes containing DK-SFM, and stored on ice until capturing. Before capturing, the cell suspension was carefully resuspended and twice passed through a 20-μm cell strainer. Cells from four independent mice, processed on two different days (two mice/day), were FACS-sorted, sequenced, and analyzed. All procedures concerning cell capturing, quality control of captured cells, single-cell cDNA synthesis, tagmentation and isolation of 5′ fragments, Illumina sequencing, processing of sequencing reads, and yield and quality of sequencing were performed as previously described (*13*).

Analysis of scRNA-seq data

The following steps were performed to analyze the single-cell mRNA sequencing data of Gli1^{+} sorted progeny (Gli1^{TOM+}). A detailed description of every step is provided in a previous study (*13*). Single-cell transcriptomes with less than 2000 unique transcriptomes were removed from the dataset before clustering. After this step, 84 transcriptomes derived from Gli1^{TOM+}/SCA-1^{+} and 97 transcriptomes from Gli1^{TOM+}/SCA-1^{-} cells remained in the dataset.

A negative binominal noise model was used to select the 2500 most variable genes. Unsupervised clustering based on Pearson correlation distances between 181 Gli1^{TOM+} single-cell transcriptomes was subsequently performed with affinity propagation. Five robust cell clusters were identified.

To identify genes that are most highly induced in TD, in comparison to IFE basal (IFE) and HF bulge cells (HFBU) (Fig. 1D), the following Bayesian negative binomial regression model was created

$$\mu = \beta_{Baseline} x_{Baseline} + \beta_{TD} x_{TD} + \beta_{IFE} x_{IFE} + \beta_{HFBU} x_{HFBU}$$

where the expression of a gene μ is modeled as the linear combination of the baseline expression predictor $\beta_{Baseline}$ that is proportional to the total number of molecules expressed in a cell and the cell type–specific binary expression predictors β_{TD}, β_{IFE}, and β_{HFBU}. Included in the model were 55 TD cells identified in the clustering of Gli1^{TOM+} cells, 228 IFE basal cells (IFE B I and IFE B II) from a previous study (*13*), and 113 HF bulge cells consisting of both Gli1^{TOM+}cells and outer bulge cells (OB III) from a previous study (13). A gene was considered induced in a population x if its population-specific predictor β_x exceeded the baseline predictor $\beta_{Baseline}$ with at least 99.9% posterior probability. Dimensionality reduction with Uniform Manifold Approximation and Projection (UMAP) was performed in Scanpy (1.8.2) (*56*).

RNA-seq analysis and data visualization

RNA-seq reads were aligned to the mouse reference genome (mm39) using STAR aligner (v2.7.9a) (*57*). Expression levels of individual genes (from the Ensembl annotation v105, both coding and noncoding) were quantified using the RSEM software (v1.3.3) to estimate counts and TPMs (transcript per million) (*58*). Differential expression analysis was performed using DESeq2 (v1.38.2) after genes with TPM < 1 in all samples were excluded. Genes reaching multiple tests adjusted P value < 0.05 and absolute fold change > 1.5 were considered to be significantly differentially expressed. The gene read counts after log transformation were also used to compute the Pearson correlation between samples, which were used for sampling clustering.

Assay for ATAC-seq library preparation, analysis, and data visualization

A total of 50,000 FACS-purified cells were collected directly into E-media. Cell sample preparation, tagmentation, and PCR amplification of tagmented DNA were done using the ATAC-seq kit (Active Motif) and following the manufacturer's instructions.

Paired-end ATAC-seq reads were trimmed with trim_galore (v0.6.7; https://github.com/FelixKrueger/TrimGalore) and then mapped to the mouse genome (mm10) using the Bowtie2 (v2.4.5; option -X 2000 –no-mixed –no-discordant) (*59*). Read pairs of mapping score > 20 were kept for analysis, and duplicated reads due to PCR amplification were removed by SAMtools (v1.9) (*60*). MACS2 (v 2.2.7.1) was used to call peaks in paired-end mode and default options (*61*). ATAC-seq peaks from all samples were merged. Reads from individual samples located at the merged peaks were computed and used for sample clustering and differential accessibility analysis using DESeq2, with significance set to false discovery rate < 5% and fold changes > 1.5. Read coverage was computed with the IGV tools and used for visualization at IGV (*62*).

Supplementary Materials

This PDF file includes:

Figs. S1 to S5

Tables S1 to S3

REFERENCES AND NOTES

1. M. Ploner, F. Schmitz, H. J. Freund, A. Schnitzler, Differential organization of touch and pain in human primary somatosensory cortex. *J. Neurophysiol.* **83**, 1770–1776 (2000).
2. L. Bai, B. P. Lehnert, J. Liu, N. L. Neubarth, T. L. Dickendesher, P. H. Nwe, C. Cassidy, C. J. Woodbury, D. D. Ginty, Genetic identification of an expansive mechanoreceptor sensitive to skin stroking. *Cell* **163**, 1783–1795 (2015).
3. S. Maksimovic, M. Nakatani, Y. Baba, A. M. Nelson, K. L. Marshall, S. A. Wellnitz, P. Firozi, S.-H. Woo, S. Ranade, A. Patapoutian, E. A. Lumpkin, Epidermal Merkel cells are mechanosensory cells that tune mammalian touch receptors. *Nature* **509**, 617–621 (2014).
4. S. M. Maricich, S. A. Wellnitz, A. M. Nelson, D. R. Lesniak, G. J. Gerling, E. A. Lumpkin, H. Y. Zoghbi, Merkel cells are essential for light-touch responses. *Science* **324**, 1580–1582 (2009).
5. Z. Halata, M. Grim, K. I. Bauman, Friedrich Sigmund Merkel and his "Merkel cell", morphology, development, and physiology: Review and new results. *Anat. Rec. A Discov. Mol. Cell. Evol. Biol.* **271**, 225–239 (2003).
6. B. A. Jenkins, N. M. Fontecilla, C. P. Lu, E. Fuchs, E. A. Lumpkin, The cellular basis of mechanosensory Merkel-cell innervation during development. *eLife* **22**, e42633 (2019).
7. M. B. Nguyen, I. Cohen, V. Kumar, Z. Xu, C. Bar, K. L. Dauber-Decker, P.-C. Tsai, P. Marangoni, O. D. Klein, Y.-C. Hsu, T. Chen, M. L. Mikkola, E. Ezhkova, FGF signalling controls the specification of hair placode-derived SOX9 positive progenitors to Merkel cells. *Nat. Commun.* **9**, 2333 (2018).
8. M. B. Nguyen, V. J. Valdes, I. Cohen, V. Pothula, D. Zhao, D. Zheng, E. Ezhkova, Dissection of Merkel cell formation in hairy and glabrous skin reveals a common requirement for FGFR2-mediated signalling. *Exp. Dermatol.* **28**, 374–382 (2019).
9. Y. S. Doucet, S.-H. Woo, M. E. Ruiz, D. M. Owens, The touch dome defines an epidermal niche specialized for mechanosensory signaling. *Cell Rep.* **3**, 1759–1765 (2013).
10. X. Sun, A. Are, K. Annusver, U. Sivan, T. Jacob, T. Dalessandri, S. Joost, A. Füllgrabe, M. Gerling, M. Kasper, Coordinated hedgehog signaling induces new hair follicles in adult skin. *eLife* **9**, e46756 (2020).
11. R. Chiquet-Ehrismann, R. P. Tucker, Tenascins and the importance of adhesion modulation. *Cold Spring Harb. Perspect. Biol.* **3**, a004960 (2011).
12. K. S. Midwood, M. Chiquet, R. P. Tucker, G. Orend, Tenascin-C at a glance. *J. Cell Sci.* **129**, 4321–4327 (2016).

13. S. Joost, A. Zeisel, T. Jacob, X. Sun, G. L. Manno, P. Lönnerberg, S. Linnarsson, M. Kasper, Single-cell transcriptomics reveals that differentiation and spatial signatures shape epidermal and hair follicle heterogeneity. *Cell Syst.* **3**, 221–237.e9 (2016).
14. H. Fujiwara, M. Ferreira, G. Donati, D. K. Marciano, J. M. Linton, Y. Sato, A. Hartner, K. Sekiguchi, L. F. Reichardt, F. M. Watt, The basement membrane of hair follicle stem cells is a muscle cell niche. *Cell* **144**, 577–589 (2011).
15. W. He, Q. Xie, Y. Wang, J. Chen, M. Zhao, L. S. Davis, M. D. Breyer, G. Gu, C.-M. Hao, Generation of a tenascin-C-CreER2 knockin mouse line for conditional DNA recombination in renal medullary interstitial cells. *PLOS One* **8**, e79839 (2013).
16. K. A. U. Gonzales, E. Fuchs, Skin and its regenerative powers: An alliance between stem cells and their niche. *Dev. Cell* **43**, 387–401 (2017).
17. E. I. Morgun, E. A. Vorotelyak, Epidermal stem cells in hair follicle cycling and skin regeneration: A view from the perspective of inflammation. *Front. Cell Dev. Biol.* **8**, 581697 (2020).
18. I. Moll, R. Paus, R. Moll, Merkel cells in mouse skin: Intermediate filament pattern, localization, and hair cycle-dependent density. *J. Invest. Dermatol.* **106**, 281–286 (1996).
19. A. Van Keymeulen, G. Mascre, K. K. Youseff, I. Harel, C. Michaux, N. De Geest, C. Szpalski, Y. Achouri, W. Bloch, B. A. Hassan, C. Blanpain, Epidermal progenitors give rise to Merkel cells during embryonic development and adult homeostasis. *J. Cell Biol.* **187**, 91–100 (2009).
20. M. C. Wright, E. G. Reed-Geaghan, A. M. Bolock, T. Fujiyama, M. Hoshino, S. M. Maricich, Unipotent, *Atoh1*$^{+}$ progenitors maintain the Merkel cell population in embryonic and adult mice. *J. Cell Biol.* **208**, 367–379 (2015).
21. Y. Xiao, D. T. Thoresen, J. S. Williams, C. Wang, J. Perna, R. Petrova, I. Brownell, Neural Hedgehog signaling maintains stem cell renewal in the sensory touch dome epithelium. *Proc. Natl. Acad. Sci. U.S.A.* **112**, 7195–7200 (2015).
22. M. C. Wright, G. J. Logan, A. M. Bolock, A. C. Kubicki, J. A. Hemphill, T. A. Sanders, S. M. Maricich, Merkel cells are long-lived cells whose production is stimulated by skin injury. *Dev. Biol.* **422**, 4–13 (2017).
23. B. U. Hoffman, Y. Baba, T. N. Griffith, E. V. Mosharov, S.-H. Woo, D. D. Roybal, G. Karsenty, A. Patapoutian, D. Sulzer, E. A. Lumpkin, Merkel cells activate sensory neural pathways through adrenergic synapses. *Neuron* **100**, 1401–1413.e6 (2018).
24. M.-G. Nunzi, A. Pisarek, E. Mugnaini, Merkel cells, corpuscular nerve endings and free nerve endings in the mouse palatine mucosa express three subtypes of vesicular glutamate transporters. *J. Neurocytol.* **33**, 359–376 (2004).
25. K. Chanda, S. Das, J. Chakraborty, S. Bucha, A. Maitra, R. Chatterjee, D. Mukhopadhyay, N. P. Bhattacharyya, Altered levels of long NcRNAs Meg3 and Neat1 in cell and animal models of huntington's disease. *RNA Biol.* **15**, 1348–1363 (2018).
26. K. Brose, K. S. Bland, K. H. Wang, D. Arnott, W. Henzel, C. S. Goodman, M. Tessier-Lavigne, T. Kidd, Slit proteins bind robo receptors and have an evolutionarily conserved role in repulsive axon guidance. *Cell* **96**, 795–806 (1999).
27. M. Ieda, K. Fukuda, Y. Hisaka, K. Kimura, H. Kawaguchi, J. Fujita, K. Shimoda, E. Takeshita, H. Okano, Y. Kurihara, H. Kurihara, J. Ishida, A. Fukamizu, H. J. Federoff, S. Ogawa, Endothelin-1 regulates cardiac sympathetic innervation in the rodent heart by controlling nerve growth factor expression. *J. Clin. Invest.* **113**, 876–884 (2004).
28. N. C. Boles, S. E. Hirsch, S. Le, B. Corneo, F. Najm, A. P. Minotti, Q. Wang, S. Lotz, P. J. Tesar, C. A. Fasano, NPTX1 regulates neural lineage specification from human pluripotent stem cells. *Cell Rep.* **6**, 724–736 (2014).
29. H. Zhang, A. S. Verkman, Aquaporin-1 tunes pain perception by interaction with $Na_v1.8$ Na^+ channels in dorsal root ganglion neurons. *J. Biol. Chem.* **285**, 5896–5906 (2010).
30. M. S. Minett, V. Pereira, S. Sikandar, A. Matsuyama, S. Lolignier, A. H. Kanellopoulos, F. Mancini, G. D. Iannetti, Y. D. Bogdanov, S. Santana-Varela, Q. Millet, G. Baskozos, R. M. Allister, J. J. Cox, J. Zhao, J. N. Wood, Endogenous opioids contribute to insensitivity to pain in humans and mice lacking sodium channel Nav1.7. *Nat. Commun.* **4**, 8967 (2015).
31. M. D. Rosenblum, E. B. Olasz, K. B. Yancey, J. E. Woodliff, Z. Lazarova, K. A. Gerber, R. L. Truitt, Expression of CD200 on epithelial cells of the murine hair follicle: A role in tissue-specific immune tolerance? *J. Invest. Dermatol.* **123**, 880–887 (2004).
32. C. S. Trempus, R. J. Morris, C. D. Bortner, G. Cotsarelis, R. S. Faircloth, J. M. Reece, R. W. Tennant, Enrichment for living murine keratinocytes from the hair follicle bulge with the cell surface marker CD34. *J. Invest. Dermatol.* **120**, 501–511 (2003).
33. K. M. Polkoff, N. K. Gupta, A. J. Green, Y. Murphy, J. Chung, K. L. Gleason, S. G. Simpson, D. M. Walker, B. Collins, J. A. Piedrahita, LGR5 marks cycling, yet long-lived, hair follicle stem cells. *Nat. Genet.* **40**, 1291–1299 (2008).
34. M. Kimura-Ueki, Y. Oda, J. Oki, A. Komi-Kuramochi, E. Honda, M. Asada, M. Suzuki, T. Imamura, Hair cycle resting phase is regulated by cyclic epithelial FGF18 signaling. *J. Invest. Dermatol.* **132**, 1338–1345 (2012).
35. A. N. Mardaryev, N. Meier, K. Poterlowicz, A. A. Sharov, T. Y. Sharova, M. I. Ahmed, V. Rapisarda, C. Lewis, M. Y. Fessing, T. M. Ruenger, J. Bhawan, S. Werner, R. Paus, V. A. Botchkarev, Lhx2 differentially regulates Sox9, Tcf4 and Lgr5 in hair follicle stem cells to promote epidermal regeneration after injury. *Development* **138**, 4843–4852 (2011).
36. Z. Xu, W. Wang, K. Jiang, Z. Yu, H. Huang, F. Wang, B. Zhou, T. Chen, Embryonic attenuated Wnt/β-catenin signaling defines niche location and long-term stem cell fate in hair follicle. *eLife* **4**, e10567 (2015).
37. H. J. Snippert, A. Haegebarth, M. Kasper, V. Jaks, J. H. van Es, N. Barker, M. van de Wetering, M. van den Born, H. Begthel, R. G. Vries, D. E. Stange, R. Toftgård, H. Clevers, *Lgr6* Marks stem cells in the hair follicle that generate all cell lineages of the skin. *Science* **327**, 1385–1389 (2010).
38. M. Weber, M. B. Nguyen, M. Y. Li, P. Flora, M. Shuda, E. Ezhkova, Merkel cell polyomavirus T antigen-mediated reprogramming in adult merkel cell progenitors. *J. Invest. Dermatol.* **143**, 2163–2176.e6 (2023).
39. P. Rompolas, K. R. Mesa, K. Kawaguchi, S. Park, D. Gonzalez, S. Brown, J. Boucher, A. M. Klein, V. Greco, Spatiotemporal coordination of stem cell commitment during epidermal homeostasis. *Science* **352**, 1471–1474 (2016).
40. A. Sada, F. Jacob, E. Leung, S. Wang, B. S. White, D. Shalloway, T. Tumbar, Defining the cellular lineage hierarchy in the interfollicular epidermis of adult skin. *Nat. Cell Biol.* **18**, 619–631 (2016).
41. S. Ghuwalewala, S. A. Lee, K. Jiang, J. Baidya, G. Chovatiya, P. Kaur, D. Shalloway, T. Tumbar, Binary organization of epidermal basal domains highlights robustness to environmental exposure. *EMBO J.* **41**, e110488 (2022).
42. P. Flora, E. Ezhkova, Regulatory mechanisms governing epidermal stem cell function during development and homeostasis. *Development* **147**, dev194100 (2020).
43. K. R. Mesa, K. Kawaguchi, K. Cockburn, D. Gonzalez, J. Boucher, T. Xin, A. M. Klein, V. Greco, Homeostatic epidermal stem cell self-renewal is driven by local differentiation. *Cell Stem Cell* **23**, 677–686.e4 (2018).
44. Y. Xiao, D. T. Thoresen, L. Miao, J. S. Williams, C. Wang, R. P. Atit, S. Y. Wong, I. Brownell, A cascade of Wnt, Eda, and Shh signaling is essential for touch dome Merkel cell development. *PLOS Genet.* **12**, e1006150 (2016).
45. M. Ito, Y. Liu, Z. Yang, J. Nguyen, F. Liang, R. J. Morris, G. Cotsarelis, Stem cells in the hair follicle bulge contribute to wound repair but not to homeostasis of the epidermis. *Nat. Med.* **11**, 1351–1354 (2005).
46. X. Sun, S. Joost, M. Kasper, Plasticity of epithelial cells during skin wound healing. *Cold Spring Harb. Perspect. Biol.* **15**, a041232 (2023).
47. S.-H. Woo, M. Stumpfova, U. B. Jensen, E. A. Lumpkin, D. M. Owens, Identification of epidermal progenitors for the Merkel cell lineage. *Development* **137**, 3965–3971 (2010).
48. S. Dekoninck, E. Hannezo, A. Sifrim, Y. A. Miroshnikova, M. Aragona, M. Malfait, S. Gargouri, C. de Neunheuser, C. Dubois, T. Voet, S. A. Wickström, B. D. Simons, C. Blanpain, Defining the design principles of skin epidermis postnatal growth. *Cell* **181**, 604–620.e22 (2020).
49. J. Feng, J. Luo, P. Yang, J. Du, B. S. Kim, H. Hu, Piezo2 channel-Merkel cell signaling modulates the conversion of touch to itch. *Science* **360**, 530–533 (2018).
50. J. Feng, Y. Zhao, Z. Xie, K. Zang, S. Sviben, X. Hu, J. A. J. Fitzpatrick, L. Wen, Y. Liu, T. Wang, K. Lawson, Q. Liu, Y. Yan, X. Dong, L. Han, G. F. Wu, B. S. Kim, H. Hu, Miswiring of Merkel cell and pruriceptive C fiber drives the itch-scratch cycle. *Sci. Transl. Med.* **14**, eabn4819 (2022).
51. A. Bataille-Savattier, C. Le Gall-Ianotto, N. Lebonvallet, L. Misery, M. Talagas, Do Merkel complexes initiate mechanical itch? *Exp. Dermatol.* **32**, 226–234 (2023).
52. S. C. Peterson, M. Eberl, A. N. Vagnozzi, A. Belkadi, N. A. Veniaminova, M. E. Verhaegen, C. K. Bichakjian, N. L. Ward, A. A. Dlugosz, S. Y. Wong, Basal cell carcinoma preferentially arises from stem cells within hair follicle and mechanosensory niches. *Cell Stem Cell* **16**, 400–412 (2015).
53. K. Thibault, Evidence of an epithelial origin of Merkel cell carcinoma. *Mod. Pathol.* **35**, 446–448 (2022).
54. A. Harold, Y. Amako, J. Hachisuka, Y. Bai, M. Y. Li, L. Kubat, J. Gravemeyer, J. Franks, J. R. Gibbs, H. J. Park, E. Ezhkova, J. C. Becker, M. Shuda, Conversion of Sox2-dependent Merkel cell carcinoma to a differentiated neuron-like phenotype by T antigen inhibition. *Proc. Natl. Acad. Sci. U.S.A.* **116**, 20104–20114 (2019).
55. S. Ahn, A. L. Joyner, Dynamic changes in the response of cells to positive hedgehog signaling during mouse limb patterning. *Cell* **118**, 505–516 (2004).
56. F. A. Wolf, P. Angerer, F. J. Theis, SCANPY: Large-scale single-cell gene expression data analysis. *Genome Biol.* **19**, 15 (2018).
57. A. Dobin, C. A. Davis, F. Schlesinger, J. Drenkow, C. Zaleski, S. Jha, P. Batut, M. Chaisson, T. R. Gingeras, STAR: Ultrafast universal RNA-seq aligner. *Bioinformatics* **29**, 15–21 (2013).
58. B. Li, C. N. Dewey, RSEM: Accurate transcript quantification from RNA-Seq data with or without a reference genome. *BMC Bioinformatics* **4**, 323 (2011).
59. B. Langmead, S. L. Salzberg, Fast gapped-read alignment with Bowtie 2. *Nat. Methods* **9**, 357–359 (2012).
60. P. Danecek, J. K. Bonfield, J. Liddle, J. Marshall, V. Ohan, M. O. Pollard, A. Whitwham, T. Keane, S. A. M. Carthy, R. M. Davies, H. Li, Twelve years of SAMtools and BCFtools. *GigaScience.* **10**, (2021).
61. J. Feng, T. Liu, B. Qin, Y. Zhang, X. S. Liu, Identifying ChIP-seq enrichment using MACS. *Nat. Protoc.* **7**, 1728–1740 (2012).
62. J. T. Robinson, H. Thorvaldsdóttir, W. Winckler, M. Guttman, E. S. Lander, G. Getz, J. P. Mesirov, Integrative genomics viewer. *Nat. Biotechnol.* **29**, 24–26 (2011).

Acknowledgments: For help and critical suggestions, we thank S. Ezhkov and all Ezhkova and Kasper lab members. We thank Hao and Fogo for the *Tnc-CreER* mice, Chen for the *Sox9-CreER* mice, and Sharifi for the *Tnc*$^{-/-}$ KO mice. We would also like to thank the Flow Cytometry Core facility at the ISMMS. **Funding:** Research reported here was supported by the National Institute of Arthritis and Musculoskeletal and Skin Diseases under award numbers R01AR063724 and P30AR079200 (to E.E.) and Department of Defense Rare Cancer Program W81XWH2110564 (to E.E.), Karolinska Institutet KID funding (to K.A. and S.J.), and the Swedish Research Council and the Swedish Cancer Society (to M.K.). X.Y.Z. is supported by the Gates Millennium Scholar's Program. **Author contributions:** Conceptualization: M.B.N., P.F., U.S., M.K., and E.E. Methodology: M.B.N., P.F., M.C.B., M.W., and U.S. Investigation: M.B.N., P.F., S.J., K.A., X.Y.Z., and D.Z. Visualization: P.F., M.B.N., X.Y.Z., K.A., D.Z., and E.E. Supervision: D.Z., M.K., and E.E. Writing—original draft: P.F., M.C.B., M.B.N., and E.E. Writing—review and editing: P.F., M.C.B., M.B.N., M.W., X.Y.Z., U.S., S.J., K.A., D.Z., M.K., and E.E. **Competing interests:** The authors declare that they have no competing interests. **Data and materials availability:** All data needed to evaluate the conclusions in the paper are present in the paper and/or the Supplementary Materials. The accession number for the bulk RNA-seq and ATAC-seq data reported in this paper is GSE228989. Sequencing data of Gli1^{TOM+} cells are deposited at Array Express under the accession number E-MTAB-6031, and the telogen full epidermis single-cell data (*13*) are deposited at NCBI GEO under the accession number GSE67602. The code for the complete analysis workflow is available at https://github.com/kasperlab and at Zenodo https://doi.org/10.5281/zenodo.10389998.

Submitted 4 May 2023
Accepted 20 December 2023
Published 19 January 2024
10.1126/sciadv.adi5791